Reactive dynamics in a deterministic thermal bath

Sanjaya Baratham, Ivan L'Heureux, and Raymond Kapral

Citation: The Journal of Chemical Physics **91**, 5602 (1989); doi: 10.1063/1.457563
View online: http://dx.doi.org/10.1063/1.457563
View Table of Contents: http://scitation.aip.org/content/aip/journal/jcp/91/9?ver=pdfcov
Published by the AIP Publishing

Reactive dynamics in a deterministic thermal bath

Sanjaya Baratham, Ivan L'Heureux, and Raymond Kapral
Chemical Physics Theory Group, Department of Chemistry, University of Toronto, Toronto, Ontario M5S 1A1, Canada

(Received 25 May 1989; accepted 3 July 1989)

A study of barrier crossing dynamics is presented for a simple two-degree-of-freedom system coupled to a Nosé–Hoover heat bath. The characteristics of the deterministic heat bath are found to give rise to a variety of rate processes. Examination of the microscopic dynamics indicates how bath fluctuations drive the reactive dynamics and gives insight into how different deterministic heat baths can be constructed to model specific bath fluctuation effects.

I. INTRODUCTION

Chemical reactions in many-body systems are often modeled by the dynamics of a special degree of freedom termed the reaction coordinate. In approximate theories the effects of the environment on the reaction coordinate are usually taken into account through the introduction of stochastic forces satisfying a fluctuation–dissipation theorem which relates the dissipation in the medium to the strength of the fluctuations that are gauged by the temperature T of the environment. Kramers' theory[1] of barrier crossing dynamics is perhaps the most widely used theory of this type.

The stochastic forces are intended to mimic the effects of the coupling of the reaction coordinate to the complex deterministic dynamics of a large number of other degrees of freedom; for instance, those associated with solvent molecules in a condensed phase reaction, or the remaining degrees of freedom in a large molecule undergoing some internal conversion process. In such circumstances the entire system is characterized by a temperature T and so the canonical ensemble is the appropriate ensemble for the study of the reaction rate.

Of course, the introduction of stochastic forces is not the only way to model the influence of a heat bath. Due to a procedure devised by Nosé[2] it is possible to consider a heat bath composed of a single additional degree of freedom and its conjugate momentum. In this scheme the equations of motion of the system plus heat bath are deterministic and time reversible. Provided the system dynamics is ergodic, the microcanonical dynamics in the extended system can yield canonical averages in the physical subsystem of interest. This is now the standard procedure for computing canonical ensemble averages of equilibrium properties from time averages in molecular dynamics. The status of dynamical properties in this scheme is less clear since the full extended system evolution is contrived to yield the equilibrium canonical distribution in the physical subsystem, but does not necessarily bear any relation to that of a physical system coupled to a real heat bath. However, in this scheme there is a great deal of flexibility in the construction of a deterministic dynamics that is consistent with an equilibrium canonical ensemble. In fact, there are infinitely many different dynamics that could be constructed,[3] so the possibility exists of exploiting this flexibility to build deterministic heat baths to mimic specific (possibly colored) noise effects on a reactive degree of freedom. So just as one might attempt to mimic a complex environment by stochastic forces, one may attempt to imitate its effects by a suitably contrived deterministic dynamics. Of course, just as one has to make choices concerning the color of the stochastic forces, decisions must be made concerning what deterministic heat bath effects are desirable.

The results presented in this paper are carried out in this spirit. While we focus on a particular heat bath choice (Nosé–Hoover dynamics[4]), studies of the type presented here could be carried out in a context that exploits the heat bath flexibility to mimic noise effects on reaction rates.

In this paper we consider a simple two-degree-of-freedom system: a reaction coordinate characterized by a bistable potential coupled to an additional oscillator degree of freedom that modifies its dynamics. This system is coupled to a Nosé–Hoover bath and the reactive dynamics is monitored. We investigate whether a chemical rate law is valid and, if so, determine the rate coefficients that characterize the transformation process. We also examine in detail the microscopic dynamics of this few-degree-of-freedom system. In many respects our investigation has goals similar to that of a previous study[5] of the microcanonical dynamics of a similar (but not identical) two-degree-of-freedom reacting system, except that we focus on canonical dynamics. A number of different types of reactive dynamics are observed for this model system indicating that the deterministic baths in this investigation can be used in place of specific colored or white noise stochastic forces. This work provides information on subsystem and bath characteristics needed for a phenomenological description of the rate process.

II. THE DYNAMICAL SYSTEM

A. Canonical dynamics

For completeness we give a brief outline of the Nosé–Hoover method for canonical ensemble molecular dynamics which essentially corresponds to a particular choice of Hamiltonian. This outline touches on some features relevant to more general schemes, such as time scaling and the relation between nonphysical (virtual) and real physical variables. This is important in order to see how dynamical properties of the system of interest are being computed and serves to illustrate the flexibility in the method referred to in Sec. I.

In this scheme the variable s and its conjugate momentum p_s are added to a nonphysical phase space $(\mathbf{q}_i,\mathbf{p}_i)$ to give an extended (virtual) system with the Nosé Hamiltonian

 0021-9606/89/215602-11$02.10

$$H = \sum_i \mathbf{p}_i^2/2m_i s^2 + V(\mathbf{q}_i) + p_s^2/2Q + gkT \ln s, \quad (1)$$

where m_i is the mass of particle i, V is the potential energy (of both the virtual and the physical system), Q is the "mass" associated with the s variable, g is a dimensionless parameter which depends on the number of degrees of freedom of the physical system and on the choice of time scaling, k is Boltzmann's constant and T is an external parameter which can be viewed as a temperature. The physical variables are introduced as

$$\mathbf{q}_i' = \mathbf{q}_i, \quad (2)$$

$$\mathbf{p}_i' = \mathbf{p}_i/s, \quad (3)$$

and these are regarded as the real physical variables. Hoover[4] scaled time by $dt' = dt/s$ and set g equal to the number of degrees of freedom f of the physical system so as to calculate canonical ensemble averages. The effect of time scaling on the phase space distribution function has been discussed by Jellinek.[6] It has also been shown that for any real g in the Hamiltonian (1) it is always possible to correspondingly adjust the time scaling so that canonical ensemble averages for the physical system at temperature T can be calculated from microcanonical averages in the extended system, provided the dynamics is ergodic. So even with a logarithmic potential for the s variable there are still infinitely many dynamics capable of producing canonical ensemble averages. In fact, the general scheme is as follows: one first uses Hamilton's equations of motion in the virtual extended system; they are then rewritten in terms of the physical and bath variables. Time scaling modifies the dynamics so that the evolving phase point samples the physical space canonically.

We apply the specific scalings given above. A simplification can be made by defining a friction-like variable, $\zeta \equiv p_s/Q$; then the scaled time equations of motion given below form a closed set:

$$\frac{d\mathbf{q}_i'}{dt'} = \frac{\mathbf{p}_i'}{m_i}, \quad (4)$$

$$\frac{d\mathbf{p}_i'}{dt'} = -\frac{\partial V}{\partial \mathbf{q}_i'} - \zeta \mathbf{p}_i', \quad (5)$$

$$\frac{d\zeta}{dt'} = \left[\sum_i \frac{\mathbf{p}_i'^2}{m_i} - fkT\right]/Q. \quad (6)$$

The phase space consists of the physical variables $(\mathbf{q}_i', \mathbf{p}_i')$ and the friction-like variable ζ. In these Nosé–Hoover equations, $(\mathbf{q}_i', \mathbf{p}_i')$ are not canonically conjugate because of the "frictional force" contribution in Eq. (5). In this phase space the distribution function

$$\rho_0 = Z^{-1} \exp\left[-\left\{V(q_i') + \sum_i p_i'^2/2m_i + Q\zeta^2/2\right\}/kT\right] \quad (7)$$

satisfies[4] $\partial\rho_0/\partial t' = 0$. Other similar thermostat forms can be used to generate the canonical distribution in physical space.[7] All the equations of motion in the following sections refer to real physical quantities so for simplicity we shall henceforth drop the primes.

B. Model for reaction dynamics

We shall apply the dynamics described above to a simple model of an isomerization reaction $A \underset{k_r}{\overset{k_f}{\rightleftharpoons}} B$ coupled to a heat bath. The potential energy of the system is chosen to be

$$V(x,y) = \tfrac{1}{2}m\omega^2 x^2 + (ay^4/4 - by^2/2)(1 - Lx + \tfrac{1}{2}L^2x^2), \quad (8)$$

where y is the reaction coordinate, x is a harmonic oscillator coordinate coupled to y through the quadratic term $(1 - Lx + \frac{1}{2}L^2x^2)$, while a, b, m, ω and L are parameters. For a fixed x, $V(x,y)$ is a symmetric bistable quartic potential. The x variable can be thought of physically to represent an intramolecular degree of freedom coupled to the reaction coordinate so as to allow energy exchange.

Scaling lengths by $\sqrt{kT/b}$, momenta by $\sqrt{mkT}$, the friction by $\sqrt{kT/Q}$ and time by $\omega_b^{-1} = \sqrt{m/b}$, where $m\omega_b^2 \equiv -(\partial^2 V/\partial y^2)|_{y=x=0}$, gives the equations of motion

$$\dot{x} = p_x, \quad (9)$$

$$\dot{y} = p_y, \quad (10)$$

$$\dot{p}_x = -\zeta p_x F + \frac{1}{2}(S - S^2x)\left(\frac{G}{4}y^4 - y^2\right) - 2Rx, \quad (11)$$

$$\dot{p}_y = -\zeta p_y F + (y - Gy^3)(1 - Sx + S^2x^2/2), \quad (12)$$

$$\dot{\zeta} = F(p_x^2 + p_y^2 - 2). \quad (13)$$

The equilibrium distribution function is

$$\rho_0 = Z^{-1} \exp[-V(x,y) - p_x^2/2 - p_y^2/2 - \zeta^2/2]. \quad (14)$$

The potential scaled by kT is

$$V(x,y) = Rx^2 + (Gy^4/4 - y^2/2)(1 - Sx + \tfrac{1}{2}S^2x^2). \quad (15)$$

Here we have introduced the parameters

$$R = \tfrac{1}{2}m\omega^2/b, \quad S = L\sqrt{kT/b}, \quad (16)$$

$$F = \sqrt{kTm/Qb}, \quad G = \frac{akT}{b^2} = \frac{kT}{4\Delta E_b}. \quad (17)$$

The parameter R is related to the frequency of the harmonic oscillator, S is a parameter coupling the molecular variable x to the reaction coordinate y, F is an adjustable coupling parameter related to the "mass" Q of the heat bath oscillator and G is related to the barrier height ΔE_b at $x = 0$. Figure 1 shows the potential energy surfaces for two sets of parameters which we will concentrate on in the rest of this study. Figure 1(a) is the surface for parameter set A where $F = 0.05$, $G = 0.07$, $R = 2.5$ and $S = 0.25$. Parameter set B is shown in Fig. 1(b) and here $F = 1.2$, $G = 0.15$, $R = 1.0$ and $S = 1.0$. The figures clearly exhibit the saddle point at (0,0) and the well regions of the potential. The potential model we have used in this study is similar to that of De Leon and Berne[5] but the nature of the oscillator and coupling term for the x variable are different. In canonical dynamics the energy of the system fluctuates and the model of Ref. 5 results in an equilibrium distribution function which can be normalized only if finite bounds are placed on the x variable. Our present model was chosen so that such arbitrary restric-

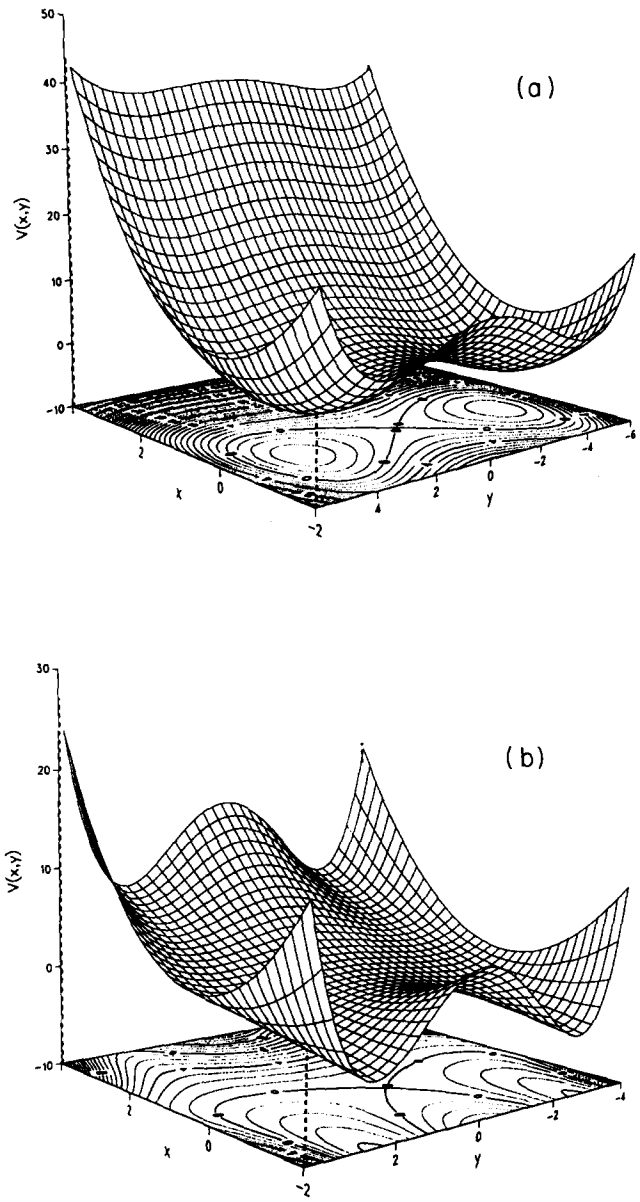

FIG. 1. The potential energy surfaces $V(x,y)$ for two different sets of parameters showing the barrier and well regions. (a) is for the parameters $F=0.05$, $G=0.07$, $R=2.5$ and $S=0.25$, while (b) is for $F=1.2$, $G=0.15$, $R=1.0$ and $S=1.0$.

tions need not be imposed, but this means that the choice of parameters cannot be arbitrary. The minimum value of $Gy^4/4-y^2/2$ is $-1/4G$ and occurs at $y=\pm 1/\sqrt{G}$. Now $V(x,1/\sqrt{G})=(R-S^2/8G)x^2+Sx/4G-1/4G$, which means we must have $R>S^2/8G$ to ensure normalization of ρ_0. This illustrates a complication which would not arise in a microcanonical study.

Insight into the coupling of the x and y variables can be gained by examining the fluctuations of the barrier height with different x values. From Eq. (15) the barrier height is $1/4G(1-Sx+\frac{1}{2}S^2x^2)$, which means that the minimum barrier height at $x=1/S$ is half the height at $x=0$. So a large value of S means that there will be large variations in the barrier height for small changes in x. This effect is clearly shown in Fig. 1, and the steepness of the barrier for the different parameter values should also be noted.

In the next section we give a brief description of dynamical quantities computed using the equations of motion given above. Viewed from another perspective, one may regard our simple two-degree-of-freedom reaction model as a probe of the nature of the Nosé–Hoover dynamics.

C. Description of reactive dynamics

As mentioned earlier one goal of this investigation is to determine the nature of the reactive dynamics as a function of system and heat bath characteristics. One question of special interest in this connection is whether a phenomenological rate law exists for some range of parameters of the model. In Ref. 5 it was concluded that there did exist parameter regimes where a phenomenological rate law existed for a microcanonical system very similar to our subsystem.

The reactive dynamics consists of the motion of a "particle" in the potential $V(x,y)$ coupled to the deterministic bath. With y as the reaction coordinate we may identify distinct chemical species with the two sides of the quartic bistable potential; hence, the chemical species dynamical variables are the Heaviside functions

$$N_A(t)=\Theta[-y(t)],N_B(t)=\Theta[y(t)]. \tag{18}$$

Normally one assumes that the averages of these species variables over an initial nonequilibrium ensemble, $\overline{N}_A$ and $\overline{N}_B$, satisfy a rate law of the form

$$\frac{d\overline{N}_A(t)}{dt}=-k_f\overline{N}_A(t)+k_r\overline{N}_B(t). \tag{19}$$

Using the regression hypothesis one may assume that the autocorrelation function of the fluctuations of the species variables in an equilibrium ensemble,

$$C(t)=\langle\delta N_A(t)\delta N_A\rangle/\langle(\delta N_A)^2\rangle \tag{20}$$

also satisfies the phenomenological rate law. Here $\delta N_A=N_A-\langle N_A\rangle$, with the angular brackets denoting an equilibrium (canonical ensemble) average over ρ_0.

The linear response theory of chemical reaction rates allows one to write molecular expressions for the rate coefficients.[8,9] If a time scale separation exists between the characteristic time for chemical relaxation between species and microscopic times characteristic of other dynamical processes in the system, so that a phenomenological rate law exists, then the rate coefficients (or chemical relaxation time) may be extracted from the plateau value of the quantity[8–10]

$$\tau^{-1}(t)=k_f(t)+k_r(t)$$
$$=(x_Ax_B)^{-1}\langle(p_y/m)\,\delta(y)\Theta[y(t)]\rangle, \tag{21}$$

while the transition state approximation follows from the $t=0^+$ value of this expression[10]:

$$\tau_{\rm tst}^{-1}=(x_Ax_B)^{-1}\langle(p_y/m)\,\delta(y)\Theta(p_y)\rangle. \tag{22}$$

In these equations x_A and x_B are the equilibrium mole fractions of A and B, respectively. The ratio of $\tau^{-1}(t)$ to its transition state value is the transmission coefficient

$$\kappa(t)=\tau^{-1}(t)/\tau_{\rm tst}^{-1}, \tag{23}$$

which contains the essential dynamical features associated with the barrier crossing reactive process.

III. RESULTS OF DYNAMICAL SIMULATIONS

A. Transmission coefficient

In this section and the next we concentrate on the two sets of parameters for which the potential energy surfaces were shown in Fig. 1. The potential energy surface for parameter set A ($F = 0.05$, $G = 0.07$, $R = 2.5$ and $S = 0.25$) displays a high but slowly rising barrier; the x oscillator has a high frequency while the bath oscillator dynamics occurs on a relatively slow time scale. For this parameter set the coupling is such that the x oscillator produces only small perturbations in the barrier height. Parameter set B has $F = 1.2$, $G = 0.15$, $R = 1.0$ and $S = 1.0$, and gives rise to a reduction of the frequency of the x oscillator and an increase of the frequency of the bath oscillator. The increased coupling between x and y means that x oscillations lead to much larger fluctuations in the barrier height. It will be seen that for parameter set B the x variable plays a much greater role in the barrier crossing dynamics, and that for set A the ζ variable almost totally controls the barrier crossing process. A detailed study for parameter set A gives much insight into the nature of the canonical dynamics and we shall also present results for intermediate parameter values in order to illustrate the transition between the two different types of behavior.

The transmission coefficient $\kappa(t)$ can be computed directly from the dynamics with initial conditions corresponding to the barrier top.[10,11] In Figs. 2(a) and 2(b) we present the reflection coefficient $\eta(t) = 1 - \kappa(t)$ vs time for the parameter sets A and B, respectively. The results were obtained from averages over an ensemble of trajectories (details of the calculation are given in the Appendix).

In Fig. 2(a) the structure of this function is rather different from that expected if the usual phenomenological description of the rate process applies: instead of a smooth increase of the "plateau" region on the chemical relaxation time scale to $\eta = 1$, the time development of η exhibits a series of plateaus. We note that the characteristic time for equilibration of the chemical concentrations is roughly 135 time units (see Sec. III B), so the stepwise evolution is occurring on this time scale. A number of other features of this curve are worth noting: there is a finite but very short initial time region where $\eta(t)$ is exactly zero [transmission coefficient $\kappa(t) = 1$], and the midregions of the plateaus are exactly constant. In Sec. III B we shall discuss the origins of these features and argue that the behavior is indicative of incipient phenomenological rate law character.

The structure of Fig. 2(b) corresponds much more closely to the usual phenomenological description of the reactive dynamics in a classical white noise heat bath. However, remnants of the stepwise evolution shown in Fig. 2(a) are still visible and there is a time region of approximately 20 time units where $\eta(t)$ is exactly zero and so no recrossings occur in this region. The coherent step-like evolution has totally disappeared after about 300 time units and $\eta(t)$ then tends towards unity on a slow time scale (which is that of chemical relaxation). For this parameter set a phenomenological rate law would fairly accurately describe the barrier crossing dynamics. This is further justified in Sec. IV where the microscopic dynamics is considered.

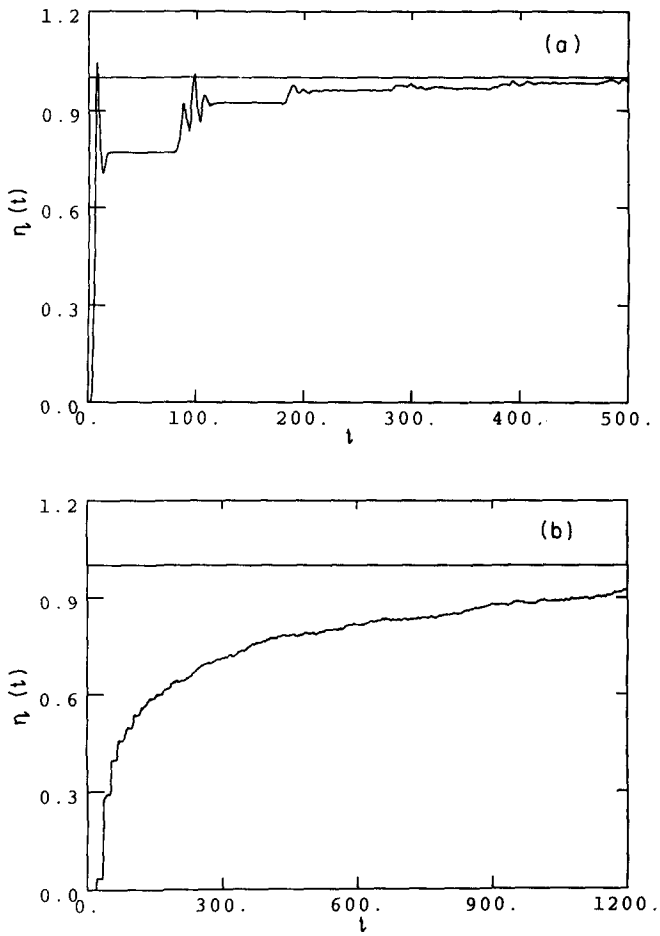

FIG. 2. (a) shows the reflection coefficient $\eta(t)$ for parameter set A where $F = 0.05$, $G = 0.07$, $R = 2.5$ and $S = 0.25$ and (b) shows the corresponding plot for parameter set B, $F = 1.2$, $G = 0.15$, $R = 1.0$ and $S = 1.0$. For both plots the finite time region where $\eta(t)$ is exactly zero is the transition state theory regime. For set A there are several plateaus whose midregions are exactly constant and the plateaus show step-like evolution to $\eta = 1$ with steps occuring approximately every 100 time units. Set B shows transient step-like evolution but then plateaus at around time 300. There is then a slow drift towards $\eta = 1$ on the time scale of chemical relaxation.

B. Concentration autocorrelation function

It is of interest to correlate the step-like behavior observed in $\eta(t)$ for parameter set A with that of the concentration autocorrelation function, Eq. (20). More specifically we consider the correlation function

$$C_*(t) = \langle \Theta[y(0)]\Theta[y(t)] \rangle, \tag{24}$$

which is related to $C(t)$ in Eq. (20) by

$$C(t) = 4C_*(t) - 1. \tag{25}$$

The results are presented in Fig. 3 and details of the calculation are given in the Appendix. Note that in contrast to the calculation of $\eta(t)$ [or $\kappa(t)$] which only requires trajectories starting at the barrier top, the evaluation of Eq. (24) entails sampling from the full distribution function ρ_0.

The correlation function $C_*(t)$ has an initial value of 1/2 in view of the symmetry of the potential in y and, if the system is mixing, should decay to a value of 1/4. However, simulations in which initial phase points are sampled from ρ_0 indicate that the system is not even ergodic. Furthermore,

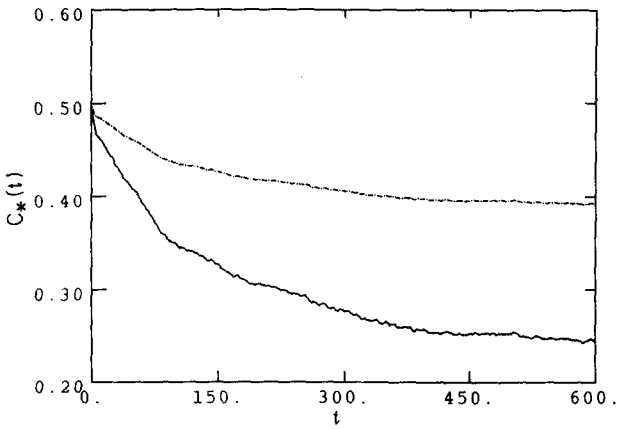

FIG. 3. The decay of the $\langle\Theta(0)\Theta(t)\rangle$ correlation function for parameter set A. In the upper dashed curve the average was performed over 15 000 trajectories while in the lower curve only the 6436 crossing trajectories were used. The decay occurs in straight line segments and for the lower curve the slopes of these segments can be correlated to the behavior of $\eta(t)$ in Fig. 2(a).

like in the investigation of De Leon and Berne, the phase space can be partitioned into phase points that lead to trajectories trapped in the wells and those that cross the barrier. It is only the latter that contribute to the ensemble used in the calculation of $\eta(t)$. Therefore, as far as reaction dynamics is concerned, it is only the measure μ_R of the phase space that corresponds to barrier crossing that is relevant. If the average in Eq. (24) is carried out over this subensemble, denoted by

$$C_R(t) = \langle\Theta[y(0)]\Theta[y(t)]\rangle_R, \tag{26}$$

then the correlation function is found to decay to 1/4, but if trapped trajectories are included in the averaging the upper dashed curve of Fig. 3 is obtained. The numerical simulations indicate that the fraction of phase points giving rise to crossing trajectories for the system parameters in Fig. 3 is $\mu_R = 0.43$.

The decay of $C_R(t)$ to its equilibrium value is not exponential, rather it consists of a series of straight line segments with different slopes; the first few segments are clearly visible in the figure. The first very short segment has a slope that characterizes the initial decay of the system: this is the transition state theory regime since no recrossings of the barrier occur in this time domain. Hence the initial slope should be given by Eq. (22) but divided by μ_R to account for the fact that we are looking at the subensemble of crossing trajectories:

$$\tau_{\mathrm{tst},R}^{-1} = 4\langle(p_y/m)\,\delta(y)\Theta(p_y)\rangle/\mu_R. \tag{27}$$

Here we used $x_A = x_B = 1/2$. The simulations confirm this prediction: the initial slope of $C_R(t)$ is 0.0057 while Eq. (27) yields 0.0063 by direct integration; these values agree within the uncertainty in the numerical simulations.

The remaining features in $\eta(t)$ and $C_R(t)$ can be correlated using the following relationship between the quantities:

$$\eta(t) = 1 - \kappa(t) = 1 + \frac{4}{\tau_{\mathrm{tst},R}^{-1}}\frac{dC_R(t)}{dt}. \tag{28}$$

Thus, the plateaus in $\eta(t)$ can be associated with the existence of linear decay segments in $C_R(t)$; in fact, the linear slopes of $C_R(t)$ can be determined and compared directly with values calculated using the plateau values in $\eta(t)$. Fitting straight lines to $C_R(t)$ from $t = 16$ to $t = 100$ and from $t = 100$ to $t = 200$ gives slopes of 0.001 32 and 0.000 47. The corresponding values obtained using Eq. (28) and the plateau values of $\eta(t)$ at times 50 and 150 are 0.001 42 and 0.000 49. These results are consistent within our error estimates.

The decay to chemical equilibrium does not follow a standard phenomenological law due to the step-like character of the time evolution of $C_R(t)$ and $\eta(t)$. We reserve a detailed discussion of the dynamical events leading to the above results for the next section but mention here that there is an intrinsic near-periodicity in the dynamics on a time scale of about 100 units. By fitting an exponential decay to the $C_R(t)$ plot, which smooths out the linear decay segments, we estimate a chemical relaxation time of 135 units, which appears consistent with the $\eta(t)$ plot. It is in this sense that we say the system shows incipient phenomenological behavior.

An analogous calculation of the concentration autocorrelation function for parameter set B was not deemed to be feasible or necessary. Such a calculation would require the integration of very long trajectories due to the fact that crossings of the barrier are infrequent events. The determination of the measure of phase space leading to crossing trajectories would be an extremely time consuming task. This is precisely the reason why the simulation starting at the barrier top is so useful in a dynamical study. Since the behavior of the transmission coefficient indicates that a phenomenological description of the reactive dynamics is approximately valid the correlation function calculation is not required in order to understand the dynamics. However, in the next section when we study the ergodic properties of the system we shall present an estimate of this correlation function from a time average along a single trajectory.

IV. MICROSCOPIC DYNAMICS

A. General features

Some insight into the step-like behavior of $\eta(t)$ for parameter set A can be obtained by examining the y distribution starting at the barrier top, $P(y,t\,|y = 0, t = 0)$, which is the conditional probability distribution of y. Figure 4 shows how this distribution evolves with time. From an examination of the figure it is clear that there is not a steady leakage of phase points between wells and, apart from transient behavior for times less than about 15 units, there is zero probability density in the barrier region for a relatively long time period during which the probability density stabilizes in the wells. At about time 80 there is again exchange between the wells that lasts until about time 120, after which there is again stabilization in the wells. This behavior is repeated periodically with the probabilities tending to their equilibrium values (symmetric about $y = 0$). The data for this evolution was obtained in the same simulation as that for the reflection coefficient calculation. The behavior of $\eta(t)$ mirrors that of $P(y,t\,|0,0)$: when there is no exchange between the wells $\eta(t)$

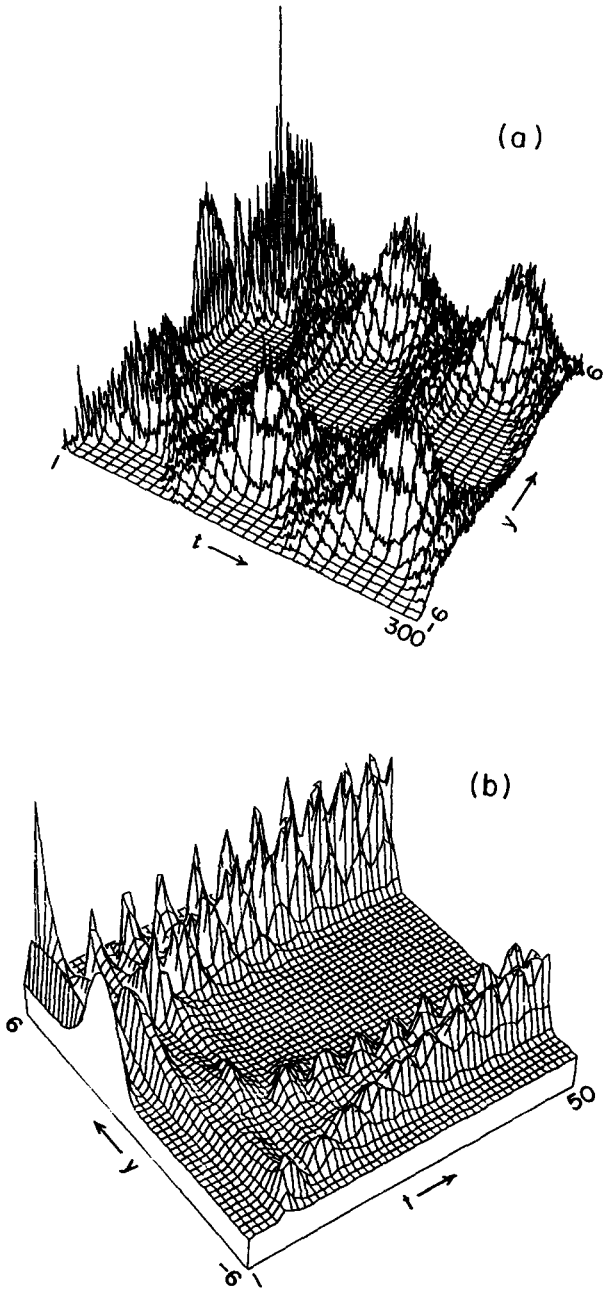

FIG. 4. Evolution of the y distribution (for parameter set A) initially constrained to be a delta function at $y = 0$, but equilibrated with respect to the other variables. Only positive values of p_y were sampled so that at very short times all of the probability density is in the product well ($y > 0$). Exchanges between the wells occur until about a time of 15 units after which the probability density stabilizes about the well minima. This corresponds to the absolutely flat initial plateau of the reflection coefficient in Fig. 2. The subsequent exchanges only occur for time regions where the reflection coefficient shows steps. (b) shows details of the evolution for the first 50 time units.

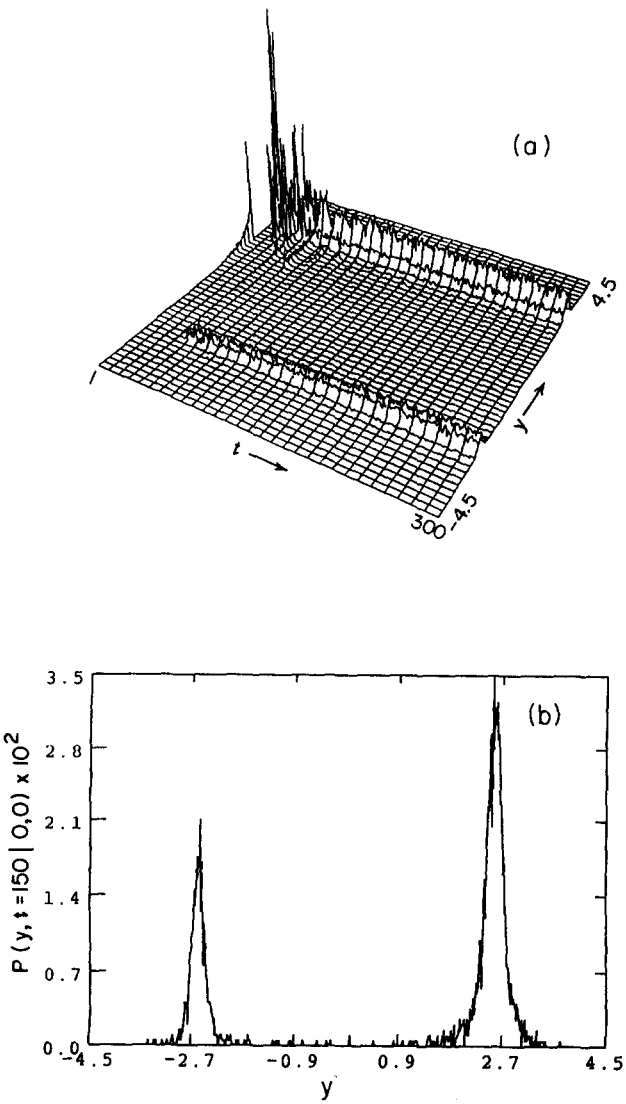

FIG. 5. Evolution of the y distribution for parameter set B, which should be contrasted to that of parameter set A in Fig. 4. The short time transient behavior is visible for times less than about 100 units. (b) shows a section taken at time 150 and illustrates the slow leakage of phase points between the wells.

is constant and the steps in $\eta(t)$ correspond to exchanges between the wells.

The evolution of $P(y,t\,|0,0)$ for parameter set B is shown in Fig. 5(a) and again it is easy to correlate this evolution with that of $\eta(t)$. Phase points first cross the barrier at about time 20 and this is where $\eta(t)$ suddenly becomes nonzero. There are regions for times less than 100 where significant probability in the barrier region is clearly visible and this corresponds to the almost vertical increases in $\eta(t)$ shown in Fig. 2(b). Figure 5(b) which corresponds to a section taken at time 150 shows that there is then a slow leakage of phase points between the wells. Figure 5(a) illustrates the transient behavior of the system and indicates that there is still some coherence in the short time dynamics. This coherence is rapidly lost and the slow leakage of phase points between the wells is exactly what would be expected in the case of a valid phenomenological rate law. The fact that the system shows transient behavior for a relatively long period could be due to an inadequacy in our definition of the chemical species dynamic variable in Eq. (18). We identify the chemical species solely through the y coordinate but interaction among the other variables in this few-degree-of-freedom system could contribute to the identification of the distinct, stable chemical species.

In addition the probability distribution for the times spent in each well was obtained. We consider the probability density $p(t)$ that the particle spends time t with y positive given that it started at the barrier top with positive momen-

tum. Figure 6(a) is for a parameter set A, Fig. 6(b) is for an intermediate parameter set ($F = 0.15$, $G = 0.15$, $R = 1.0$ and $S = 1.0$) while Fig. 6(c) is for parameter set B. For parameter set A, Fig. 6(a) clearly illustrates the gross periodicity of the reactive event. The particle has a high probability of making a short time recrossing after which the probability density is effectively zero, except for times which are integral multiples of roughly 100 time units. As expected, Fig. 6(c) shows sharp peaks from around time 20 to 100 due to the coherent nature of the first recrossings but then the probability shows a steady decay. The intermediate parameter value illustrates the transition between the two types of crossing behavior. It is interesting to contrast the decays in Fig. 6 to that which would be expected using stochastic dynamics. The simple Langevin equation with a Gaussian white noise term should show a recrossing time probability with a monotonic fall-off tending asymptotically to zero, similar to the decay in Fig. 6(c) from time 150 onwards, or the decay of the peak heights of the other two distributions. The "periodicity" in the decay is a feature peculiar to Nosé–Hoover dynamics for a slowly varying heat bath oscillator. However, one can tune the dynamics so as to reduce the "period" until eventually a temporally smooth reactive process is obtained. For our model the tuning was accomplished by simply changing the model parameters but one can envision cases where this may not be possible. To provide realistic simulations of other nonequilibrium systems the full flexibility in the choice of the dynamics may have to be exploited, and the ability to carry out such a tuning procedure will depend on the nature of the subsystem dynamics and the manner in which the deterministic bath is introduced.[3,7]

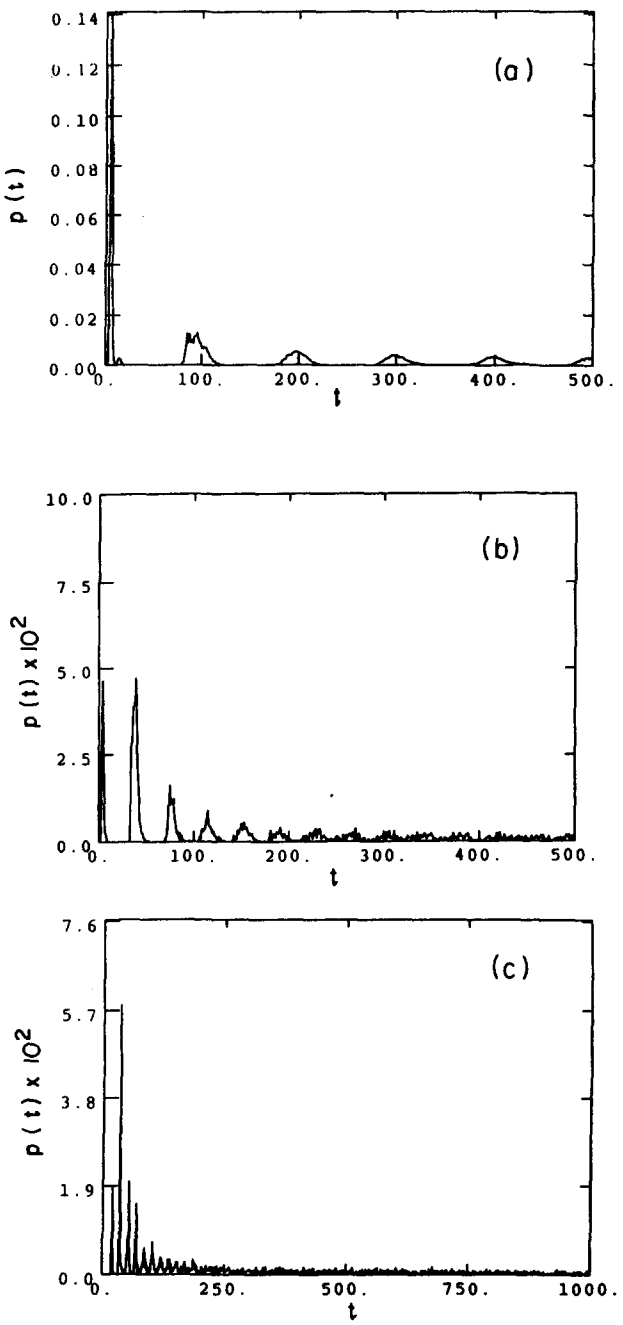

FIG. 6. (a) shows the distribution of times spent in the $y > 0$ well for parameter set A averaged over an ensemble of trajectories starting at the barrier top. There is a high probability of making a short time recrossing which corresponds to a rapid increase in the reflection coefficient. The regions of nonzero probability show peaks centered about integral multiples of the "period" time of 100 units. (b) shows the distribution for the parameter values $F = 0.15$, $G = 0.15$, $R = 1.0$, $R = 1.0$ and illustrates the transition to that of parameter set B in (c). Apart from short time transient behavior the curve in (c) is roughly similar to what would be expected using stochastic dynamics with a white noise heat bath.

We may also examine the statistical distribution of first crossing times for parameter set A with initial states sampled from the equilibrium distribution ρ_0. This distribution is given in Fig. 7 and was obtained in the same simulation as $C_R(t)$ by determining when the evolving phase points first crossed the barrier. There is a very rapid initial fall-off followed by approximately constant steps of roughly 100 time units, so again the periodicity of the system is evident. This plot gives information about the time rate of change of $C_R(t) = \langle \Theta[y(0)]\Theta[y(t)] \rangle_R$. To see this consider the simple hypothetical situation where no recrossings occur and the first crossing probability is uniformly distributed on, say, 0 to T and equal to $\bar{p}$. Then, due to the symmetry of the double well, the initial value of $C_R(t)$ is 1/2 and will decrease steadily up

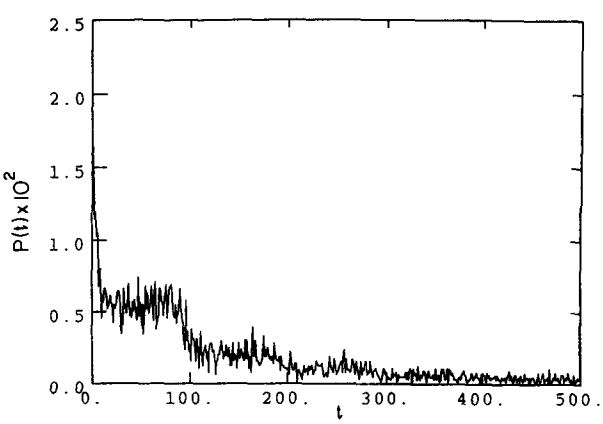

FIG. 7. The first crossing time distribution for parameter set A, obtained in the same simulation as Fig. 3, with initial points sampled from the full equilibrium distribution function. There is high probability for making a short time first crossing followed by approximately constant steps.

to time T since crossing trajectories are "absorbed" when they cross the barrier. The uniform distribution of crossing times means $C_R(t)$ will decay as

$$C_R(t) = (1 - \bar{p}t)C_R(0), \quad 0 < t < T. \tag{29}$$

Of course, consideration must also be given to recrossings (in fact, multiple recrossings) which for our system means $C_R(t)$ eventually decays to 1/4 [$\delta N_B(0)$ and $\delta N_B(t)$ are uncorrelated]. That $C_R(t)$ is still observed to decay in linear segments results from the fact that recrossings only occur at discrete times which correspond to the points where the slope of $C_R(t)$ changes. If the dynamics corresponding to crossing trajectories is ergodic, then the recrossing probabilities that need to be considered are exactly the $p(t)$ shown in Fig. 6(a).

B. Ergodic properties

For parameter set A it is of interest to examine the ergodic properties of the system in the context of the $\langle \Theta(0)\Theta(t) \rangle$ correlation function considered above. We already noted that the full system dynamics is certainly not ergodic since trajectories can be divided into those that cross the barrier and those that are confined to the well regions. In order to study the ergodicity of the reactive dynamics we computed the correlation function

$$C_T(t) = \frac{1}{T}\int_0^T dt'\, \Theta(t')\Theta(t'+t), \tag{30}$$

by performing a time average over a single crossing trajectory with arbitrarily chosen initial conditions. The maximum Lyapunov exponents for sample crossing and noncrossing trajectories were computed[12] and both appear to converge to about 0.03; Fig. 8(a) shows the results of a calculation of the maximum Lyapunov exponent $\lambda_{\max}$ for a sample crossing trajectory.

The results of the time average calculation are shown in Fig. 9 for two different initial conditions, with the averages being performed over $T = 10^6$ timesteps. Assuming that $T = 10^6$ is large enough, these calculations suggest that $C_T(t)$ depends on the initial conditions and is not identical with $C_R(t)$ computed from an ensemble averge over ρ_0 (see Fig. 3), and so implies the dynamics is not ergodic. However, the basic structure of the curves is the same as the ensemble average of Fig. 3; note in particular the decay through a sequence of linear segments. A given initial condition can give rise to a broken symmetry trajectory which does not spend equal times on the two sides of the barrier; however, different initial conditions can give rise to trajectories that show opposite preferences for a particular side of the barrier. The ensemble average $C_R(t)$ in Fig. 3 shows the decay from 0.5 to 0.25 which suggests the two kinds of broken symmetry trajectories have equal weights in ρ_0.

The correlation function $C_T(t)$ for parameter set B is shown in Fig. 10. The decay appears fairly consistent with simple exponential fall-off and fitting the data to $C_T(t) = 0.25\exp(-t/\tau) + 0.25$ gives a chemical relaxation time τ of 1125 time units. In addition, Fig. 8(b) shows that the maximal Lyapunov exponent $\lambda_{\max}$ for this parameter set converges to about 0.08 indicating chaotic dynamics. However, it should be remembered that the system shows transient decay for the first few hundred time steps and our comments in Sec. IV A concerning the chemical species dynamical variable should be noted.

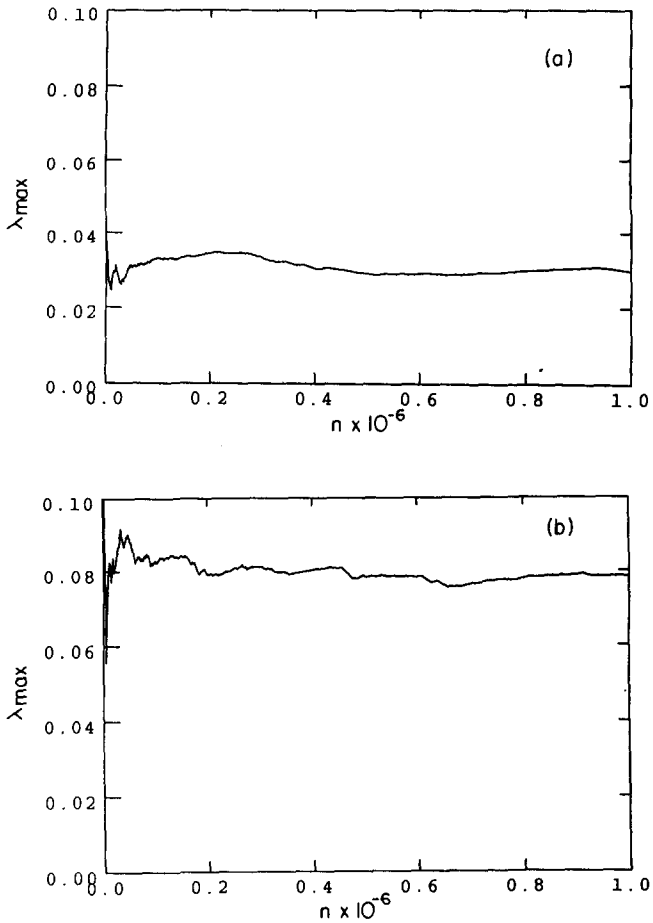

FIG. 8. Maximum Lyapunov exponent $\lambda_{\max}$ vs the number of iterations n for two sample crossing trajectories. (a) corresponds to parameter set A and $\lambda_{\max}$ converges to 0.03, while (b) for parameter set B has a $\lambda_{\max}$ which is more than twice as large.

C. Phase space trajectories

The effect of varying the parameters on the phase space trajectories has been fairly extensively investigated. The crossing trajectories are the ones of primary interest and, for a given set of parameter values, these trajectories have an overall structure which is independent of the initial conditions. Figure 11 shows both y and ζ vs time for parameter set A. The same quantities are plotted in Fig. 12 for $F = 0.25$, $G = 0.15$, $R = 1.5$ and $S = 0.5$ while Fig. 13 shows the trajectories for parameter set B. It is clear from an examination of these figures that increasing F decreases the time scale for the oscillatory motion in the friction-like variable ζ. In Fig. 11 the time variations of these variables are closely correlated and the deviations of y from the position of a stable minimum in the potential seem to follow the oscillations of the friction. Examination of the equations of motion, Eqs. (10)–(13), indicates that a negative ζ corresponds to increasing p_y while a positive ζ should produce damping effects. This is

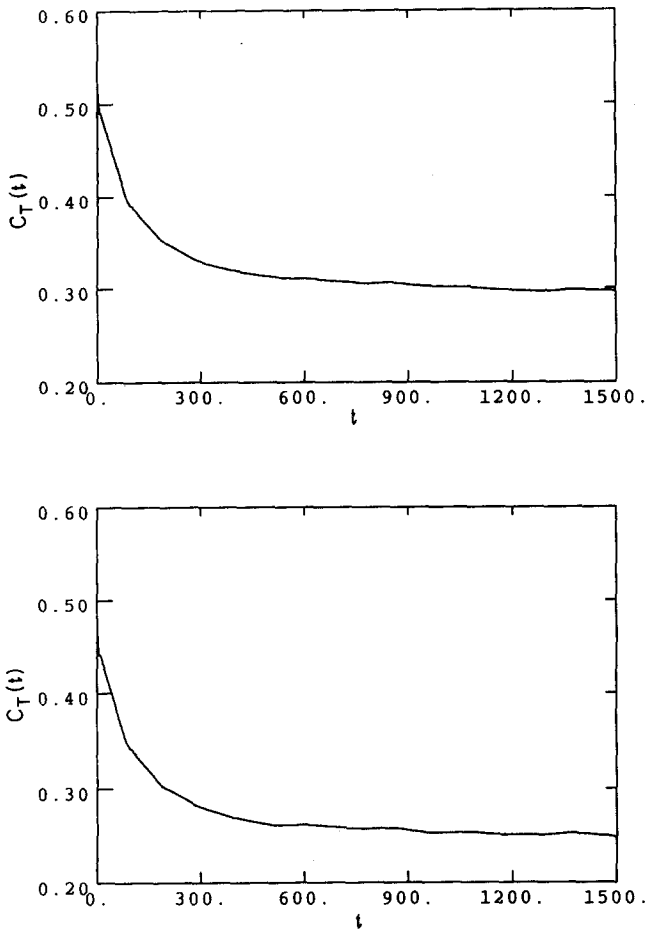

FIG. 9. The correlation function $C_T(t)$ for parameter set A showing the effect of changing the initial conditions. The structure of the curves are the same as the ensemble average in Fig. 3, but the initial and asymptotic values may be different suggesting a broken symmetry in the dynamics.

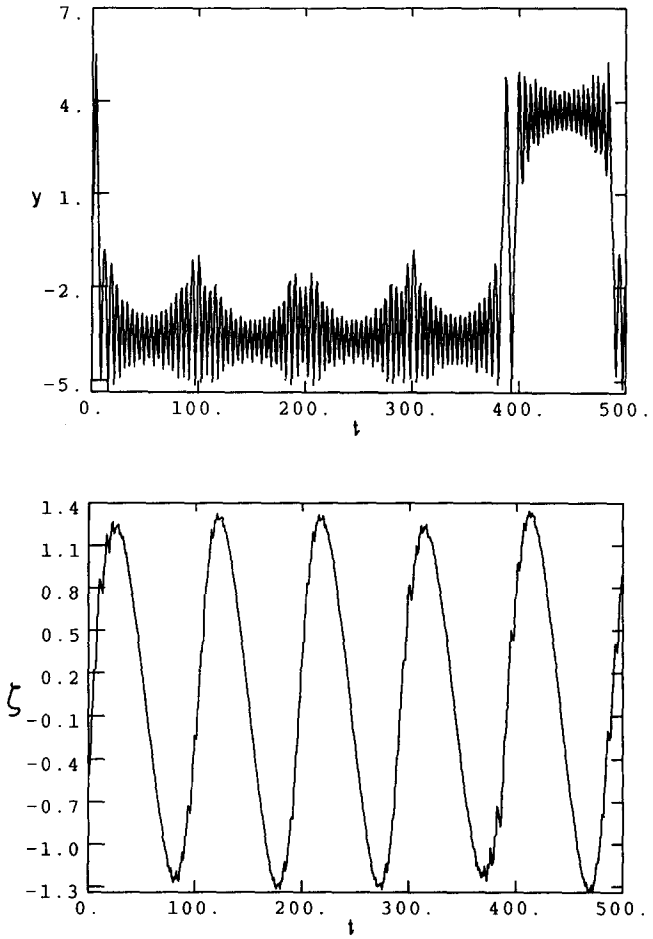

FIG. 11. Variation of y and ζ along a trajectory for the parameter set A, $F = 0.05$, $G = 0.07$, $R = 2.5$ and $S = 0.25$. The figure shows that y exhibits large deviations from the position of a well minimum only after ζ has undergone a half cycle through negative values, so the behavior of y seems to follow that of ζ.

indeed the case and the figures show it is the time region where $|\zeta|$ is small and $\dot{\zeta} > 0$ (that is, ζ has undergone a half cycle through negative values) that large oscillations in y are produced about a stable well position. On the other hand, the

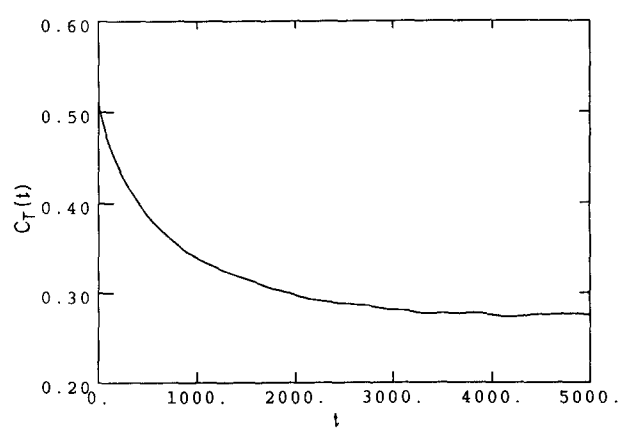

FIG. 10. The correlation function $C_T(t)$ for parameter set B computed along a trajectory whose initial conditions gave rise to a maximal Lyapunov exponent of 0.08. This curve decays on the time scale of chemical relaxation which was found to be 1125 time units.

y oscillations are minimum after ζ has completed a half cycle through positive values. In the former case, whether or not a crossing occurs must obviously depend on the other system variables but we find that x, p_x and p_y all show extremely rapid oscillations, so for this parameter set it is essentially the periodic variation of ζ which controls the reactive dynamics.

The situation in Fig. 12 shows that some of this coherence has been lost and Fig. 13 corresponds much more closely to a white noise heat bath. Here the x variable plays a much greater role in determining the barrier crossing behavior of the system and in addition much of the periodic nature of the crossings has been removed by increasing the frequency of oscillation of ζ.

V. CONCLUSION

Constant temperature barrier crossing dynamics in a few-degree-of-freedom system coupled to a deterministic heat bath can exhibit a number of different features depending on the values of the model parameters. We investigated a parameter set (A) where the transmission coefficient showed step-like evolution but was nevertheless indicative of

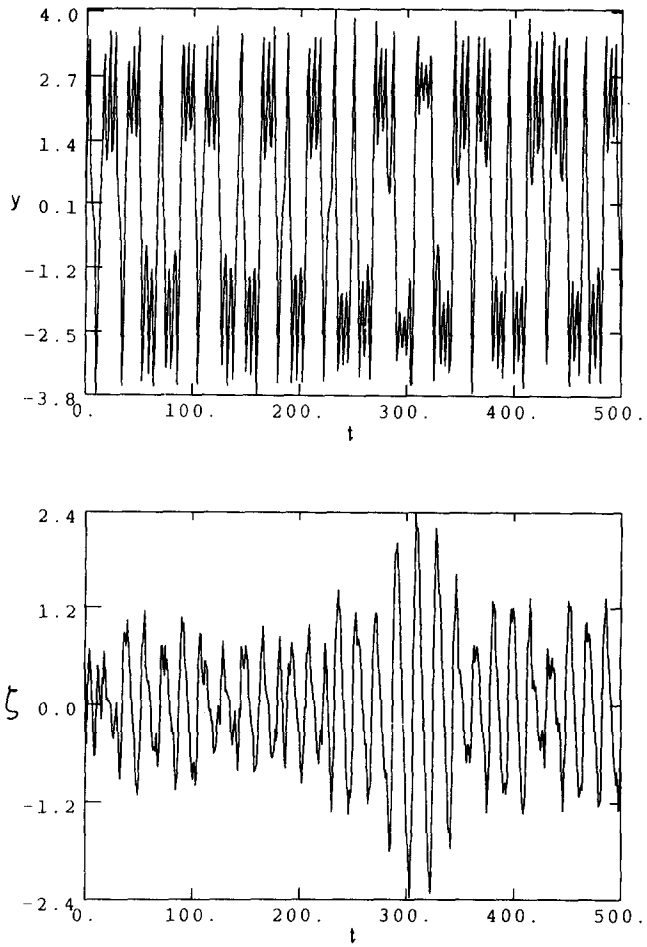

FIG. 12. Same as Fig. 11 for an intermediate parameter set, $F = 0.25$, $G = 0.15$, $R = 1.5$, $S = 0.5$. The correlations between the variations in Fig. 11 are not so apparent in this case.

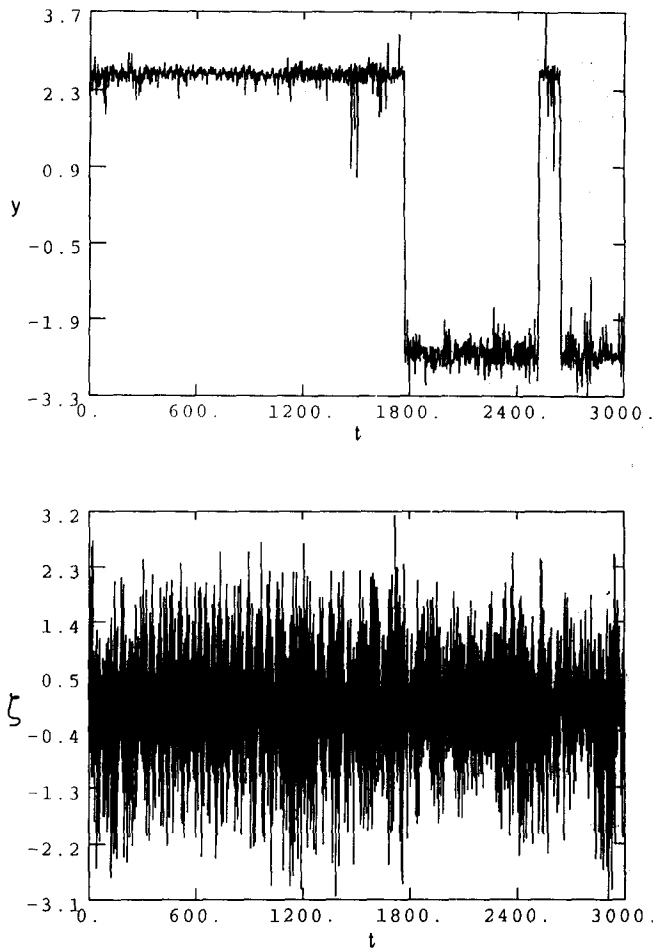

FIG. 13. Same as Fig. 11 for parameter set B, $F = 1.2$, $G = 0.15$, $R = 1.0$, $S = 1.0$. The correlations seen in Fig. 11 are not apparent here. The change is brought about by increasing the bath frequency and changing the coupling between y and x so that the x variable plays a greater role in the barrier crossing dynamics.

phenomenological character is a discrete time sense. By tuning the parameters (B) we were able to remove this stepwise evolution and obtain a system which obeyed a much more standard phenomenological rate law. In the Nosé scheme a dynamics is contrived to yield a canonical equilibrium distribution for the physical subsystem. Provided the full system dynamics is ergodic the equilibrium properties of the physical subsystem are correctly described and previous studies[2] indicate that these properties are rather insensitive to the "mass" Q which appears in the Nosé Hamiltonian [Eq. (1)]. However, the dynamics of the physical subsystem is very sensitive to this parameter. For parameter set A in our few-degree-of-freedom system, calculations show that the dynamics is not ergodic and has a periodic structure which is not like that of a system coupled to a classical white noise bath. This periodicity was also found for a simpler reactive model, without the x variable oscillator, where again steplike behavior for the transmission coefficient was observed. In view of the fact that parameter set A corresponds to weak coupling between y and x this is understandable. These features of the barrier crossing dynamics were connected to the roughly sinusoidal variation of the friction variable about a mean value of zero. For any initial value of ζ and the position y, the variation of these variables very quickly become correlated, and the deviations of y from the stable minima are controlled essentially by the oscillations in ζ. As a result the barrier crossing event has an intrinsic periodicity which implies that a great deal of the random aspects are lost. Therefore, a standard phenomenological description of the reactive dynamics was not found to be applicable. Nevertheless, certain features closely related to a phenomenological description were observed and it is possible that changing the deterministic heat bath may alter the dynamics even for the potential form corresponding to parameter set A so that it is more like a system in a classical white noise bath. Of course, in specific applications there is no reason to expect that a white noise bath is appropriate and the introduction of coherences like those seen here may be desired.

In our model, barrier crossing is governed by fluctuations in x and ζ, but for parameter set A, ζ exerts the dominant influence. Of course, in studying a bath-fluctuation-induced barrier crossing one must expect the details of the bath dynamics to play an essential role. By adjusting the parameters to set B, the x variable was allowed to play a much greater role in the barrier crossing process and the periodic nature of the reaction was almost completely removed by increasing the frequency of the ζ oscillations; note,

however, there are still unusual coherent barrier crossing which occur at short times [cf. Figs. 5 and 6(c)]. Here the bath characteristics are much more like a white noise bath and there is a fairly clear separation of time scales, which means that a phenomenological description would be approximately valid for this parameter set.

This work has provided some insight into how the single Nosé–Hoover bath can drive reactive dynamics in a small system, and could serve as a basis for constructing different deterministic heat bath models to explore specific bath fluctuation effects. In addition, the work has illustrated some features of Nosé dynamics.

ACKNOWLEDGMENTS

This research was supported in part by grants from the Natural Sciences and Engineering Research Council of Canada (NSERC) and the Petroleum Research Fund administered by the American Chemical Society. Grants of Cray time from NSERC and the Research Board of the University of Toronto are also acknowledged. We benefitted from stimulating conversation with Giovanni Ciccotti. We would also like to thank David Brown for help in constructing some of the figures.

APPENDIX

1. Evaluation of the transmission coefficient

Using time reversal symmetry, Eq. (23) for the transmission coefficient can be written

$$\kappa(t) = \frac{\langle p_y \delta(y) \Theta(p_y) [\Theta[y(t)] - \Theta[y(-t)]] \rangle}{\langle p_y \delta(y) \Theta(p_y) \rangle}, \tag{A1}$$

where the average is performed over ρ_0. By evaluating the integral in the denominator and performing the y integration in the numerator this can be written as

$$\kappa(t) = \int_{-\infty}^{\infty}\int_{-\infty}^{\infty}\int_{-\infty}^{\infty}\int_{0}^{\infty} \omega(t) \frac{e^{-Rx^2} e^{-p_x^2/2} e^{-\zeta^2/2}}{(\pi/R)^{1/2}(2\pi)^{1/2}(2\pi)^{1/2}} \times p_y e^{-p_y^2/2}\, dx\, dp_x\, d\zeta\, dp_y, \tag{A2}$$

where $\omega(t) = \{\Theta[y(t)] - \Theta[y(-t)]\}$. Defining $dv = -p_y \exp[-p_y^2/2]\, dp_y$, and $p_y = (-2\ln v)^{1/2}$ enables initial values of p_y to be obtained by sampling v uniformly on [0,1], while the initial values of x, p_x and ζ may be sampled from the normalized Gaussian distributions in Eq. (A2). Constraining y at the barrier top and using these initial values, trajectories were generated and $w(t)$ was averaged over an ensemble of such trajectories in order to compute $\kappa(t)$.

2. Evaluation of $C_R(t)$

To compute $C_*(t)$ of Eq. (24) we need to sample initial conditions from ρ_0 of Eq. (14). The initial values of p_x, p_y, and ζ are sampled from standard Gaussian distributions while x and y are sampled from

$$\rho' = Z_*^{-1} \exp[-V(x,y)] \tag{A3}$$

with

$$Z_* = 2\int_{-\infty}^{\infty}\int_{0}^{\infty} \exp[-V(x,y)]\, dx\, dy. \tag{A4}$$

Due to the symmetry of the potential in y, only positive y values need to be sampled. The sampling was performed using the Metropolis Monte Carlo algorithm. The quantity $\Theta[y(t)]$ was averaged over the ensemble of trajectories generated. In the computation of $C_R(t)$ only crossing trajectories were used in the ensemble average.

[1] H. A. Kramers, Physica 7, 284 (1940).
[2] S. Nosé, Mol. Phys. **52**, 255 (1984).
[3] J. Jellinek and R. S. Berry, Phys. Rev. A **38**, 3069 (1988).
[4] W. G. Hoover, Phys. Rev. A **31**, 1695 (1985).
[5] N. De Leon and B J. Berne, J. Chem. Phys. **75**, 3495 (1981).
[6] J. Jellinek, J. Phys. Chem. **92**, 3163 (1988).
[7] W. G. Hoover, *Molecular Dynamics* (Springer, Berlin/Heidelberg, 1986).
[8] T. Yamamoto, J. Chem. Phys. **33**, 281 (1960).
[9] See, for instance, R. Kapral, Adv. Chem. Phys. **48**, 71 (1981); J. T. Hynes, in *Theory of Chemical Reaction Dynamics*, edited by M. Baer (CRC, Boca Raton, FL, 1985), Vol. 4.; D. Chandler, *Introduction to Modern Statistical Mechanics* (Oxford University, New York, 1987).
[10] D. Chandler, J. Chem. Phys. **68**, 2959 (1978).
[11] B. J. Berne, in *Multiple Time Scales*, edited by J. U. Brackbill and B. J. Cohen (Academic, New York, 1985).
[12] G. Benettin, L. Galgani, A. Giorgilli, and J. M. Strelcyn, Meccanica **15**, 21 (1980).